



# CHORUS

This is the accepted manuscript made available via CHORUS. The article has been published as:

## Topological spin Hall effects and tunable skyrmion Hall effects in uniaxial antiferromagnetic insulators

Matthew W. Daniels, Weichao Yu (□□□), Ran Cheng, Jiang Xiao (□□), and Di Xiao

Phys. Rev. B **99**, 224433 — Published 28 June 2019

DOI: [10.1103/PhysRevB.99.224433](https://doi.org/10.1103/PhysRevB.99.224433)

# Topological spin Hall effects and tunable skyrmion Hall effects in uniaxial antiferromagnetic insulators

Matthew W. Daniels,<sup>1,2,\*</sup> Weichao Yu (余伟超),<sup>3</sup> Ran Cheng,<sup>1,4</sup> Jiang Xiao (萧江),<sup>3,5</sup> and Di Xiao<sup>1</sup>

<sup>1</sup>*Department of Physics, Carnegie Mellon University, Pittsburgh, PA 15213, USA*

<sup>2</sup>*Institute for Research in Electronics and Applied Physics,  
University of Maryland, College Park, MD 20742, USA*

<sup>3</sup>*Department of Physics and State Key Laboratory of Surface Physics, Fudan University, Shanghai 200433, China*

<sup>4</sup>*Department of Electrical and Computer Engineering,  
University of California, Riverside, CA 92521, USA*

<sup>5</sup>*Institute for Nanoelectronics Devices and Quantum Computing, Fudan University, Shanghai 200433, China*

Recent advances in the physics of current-driven antiferromagnetic skyrmions have observed the absence of a Magnus force. We outline the symmetry reasons for this phenomenon, and show that this cancellation will fail in the case of spin polarized currents. Pairing micromagnetic simulations with semiclassical spin wave transport theory, we demonstrate that skyrmions produce a spin-polarized transverse magnon current, and that spin-polarized magnon currents can in turn produce transverse motion of antiferromagnetic skyrmions. We examine qualitative differences in the frequency dependence of the skyrmion Hall angle between ferromagnetic and antiferromagnetic cases, and close by proposing a simple skyrmion-based magnonic device for demultiplexing of spin channels.

## I. INTRODUCTION

Skyrmions have long been appreciated in the magnetism community for their topological stability<sup>1</sup> and solitonic dynamics.<sup>2</sup> In metallic ferromagnets, skyrmions cause a transverse deflection of itinerant electrons known as the topological Hall effect.<sup>3</sup> When the current is strong enough to drive ferromagnetic skyrmions, the skyrmion itself undergoes motion transverse to the current; this reciprocal process is the skyrmion Hall effect. These two effects are related through conservation of momentum.<sup>4</sup> Similar effects exist in insulating magnets, where magnons, rather than electrons, represent the low-lying excitations of the system.<sup>5-7</sup>

Recently, skyrmions in metallic antiferromagnets have garnered attention as an attractive alternative to their ferromagnetic counterparts. Unlike ferromagnetic skyrmions, antiferromagnetic skyrmions do not undergo transverse motion in response to electronic current.<sup>8-10</sup> The crucial difference is the two-sublattice structure of the antiferromagnet: though each ferromagnetic sublattice nominally experiences a Magnus force, there is a perfect cancellation between the two, and the skyrmion moves only longitudinally with the current. This absence of the skyrmion Hall effect in antiferromagnets has been lauded for the resulting simplicity of the skyrmion dynamics. It may represent a significant technological advantage in the quest for spin texture based applications such as racetrack memory<sup>11</sup> or skyrmion computing.

To date, less has been said about antiferromagnetic skyrmions in insulating systems, and whether or not skyrmion Hall effects arise therein. In this paper, we explore how a magnon/skyrmion *spin* Hall effect appears in antiferromagnetic magnon-skyrmion interactions. A crucial feature of spin waves in easy axis antiferromagnets is that they are spin-polarized in general. This is expected theoretically,<sup>12,13</sup> and such magnon-mediated spin cur-

rents have recently been observed experimentally in materials such as Cr<sub>2</sub>O<sub>3</sub> and MnPS<sub>3</sub>.<sup>14,15</sup> A consequence of these spin polarized currents, and the topic of the present article, is that the perfect cancellation of Magnus forces discussed in previous works<sup>8,9,16,17</sup> does not always hold in magnonics. We present theory and simulation demonstrating how one can generate magnonic forces on antiferromagnetic skyrmions, and how, conversely, one can use skyrmions as spin-splitters in antiferromagnetic magnon devices.

In Sec. II, we justify these claims by presenting general symmetry arguments. In Sec. III, we discuss the theoretical framework underlying the rest of the paper. Sec. IV presents semiclassical transport results, supported by simulation, to describe the magnonic topological spin Hall effect generated by antiferromagnetic skyrmions. Sec. V derives the equations of motion of the skyrmion texture in this coupled system, demonstrating in simulation an angle-tunable skyrmion Hall effect. We conclude in Sec. VI by describing some possible applications of these effects in magnonic logic.

## II. SYMMETRY CONSIDERATIONS AND SUMMARY OF RESULTS

We wish to study in antiferromagnets how spin waves interact with skyrmion configurations of the antiferromagnetic order parameter. A skyrmion in a 3-dimensional<sup>18</sup> field  $\mathbf{n}(\mathbf{r})$  over a 2-dimensional plane is characterized by two criteria: it has a finite and nonzero characteristic length scale;<sup>19</sup> and it has nonzero topological charge,

$$Q = \frac{1}{4\pi} \int_{\mathbb{R}^2} \hat{n} \cdot \left( \frac{\partial \hat{n}}{\partial x} \times \frac{\partial \hat{n}}{\partial y} \right) dx dy. \quad (1)$$

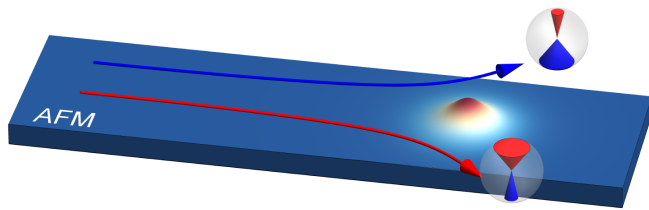


FIG. 1. This diagram shows a skyrmion, far right, subject to spin unpolarized magnon current entering from the far left. The blue and red arrows representing left- and right-handed spin wave channels have equal amplitude. Mirror symmetry about the major axis of the strip is preserved, since the  $m_z$  carried by each spin wave channel changes sign under the mirror operation. The presence of this mirror symmetry protects the skyrmion from any forces transverse to the mirror symmetry axis. If the spin accumulation becomes asymmetric across this axis (as in the left and right panels of Fig. 2), then a transverse skyrmion Hall will necessarily manifest.

Under the assumption that  $\hat{n}$  has a uniform boundary condition at infinity, it is straightforward to show that  $Q$  is quantized and that it labels topologically protected configurations of  $\hat{n}$ .<sup>1</sup> In ferromagnetic spintronics, the unit vector  $\hat{n}$  in Eq. (1) is taken to be the local magnetization vector.<sup>20</sup> In antiferromagnets, we instead take  $\hat{n} = \mathbf{n}/\|\mathbf{n}\|$  to be the normalized staggered order vector  $\mathbf{n} = (\mathbf{m}_A - \mathbf{m}_B)/2$ , defined as the local difference between sublattice magnetizations.<sup>21</sup> Though skyrmion-like bubble states can be stabilized by dipolar interactions in ferromagnets, we obviously lack this mechanism in antiferromagnets. Here, and in many ferromagnets of interest as well, our skyrmions are stabilized entirely by the competition between magnetocrystalline anisotropy and the Dzyaloshinskii-Moriya interaction in the presence of the exchange interaction. The Dzyaloshinskii-Moriya interaction arises due to inversion symmetry breaking,<sup>22</sup> either in the crystal lattice itself or due to interfaces between the magnet and another material. Because the antiferromagnetic free energy in terms of  $\mathbf{n}$  has a similar form at leading order to the ferromagnetic free energy in  $\mathbf{m}$ , many results on the stationary stabilization of ferromagnetic skyrmions<sup>23,24</sup> are expected to translate qualitatively to the antiferromagnetic case.

In ferromagnets, it is known that the emergent magnetic field of a skyrmion produces a transverse force on electronic current. In recent literature on antiferromagnetic skyrmions, the absence of an observed skyrmion Hall effect has often been explained by a simple model treating a ferromagnetic skyrmion per sublattice.<sup>8,9,17</sup> In this picture, the two ferromagnetic skyrmions have opposite skyrmion numbers and opposite emergent magnetic fields. Each ferromagnetic skyrmion thereby feels an oppositely signed Magnus force, and as the two are bound together by exchange coupling, the full antiferromagnetic skyrmion feels no net transverse force at all.

Despite this cancellation of transverse forces acting on the skyrmion, there is no reason to believe that individual

electrons feel no transverse force. A force perpendicular to a particle’s trajectory represents the breaking of mirror symmetry across the plane normal to that force. A particle that couples to a spin texture will see this mirror symmetry broken in the presence of a skyrmion, and so we expect a transverse force to appear in general. Semiclassical transport theory predicts<sup>25</sup> just such an emergent Lorentz force on electrons due to the emergent magnetic field  $\hat{n} \cdot (\partial_x \hat{n} \times \partial_y \hat{n})$  of an antiferromagnetic skyrmion, and recent first principles calculations have suggested the existence of a spin Hall effect for electrons flowing through metallic antiferromagnetic skyrmions.<sup>26</sup> Similar suggestions are also starting to be understood in ferrimagnetic systems near compensation.<sup>27</sup>

Yet so long as an equal number of spin up and spin down carriers participate in such a spin Hall effect, mirror symmetry of the spin accumulation across the direction of current flow is preserved. This also corresponds to a mirror symmetry of the spin current channels, as in Fig. 1. As such, the skyrmion itself is protected by symmetry from experiencing transverse forces; any such force would break the mirror symmetry. This explains the absence of a skyrmion Hall effect as observed in antiferromagnetic simulations,<sup>17</sup> but we emphasize that the symmetry protection holds only when the incoming current is spin unpolarized.<sup>28</sup> We also note that a proper analysis of the spin current or spin accumulation distribution has both a vector nature (in the current or position component) and pseudovector or axial nature (in the spin component).<sup>29</sup> Symmetry analysis that attempts to use the “mean” spin current in one direction or another will give incorrect results in the general case.

Magnonic excitations are also subject to these symmetry arguments; since a skyrmion breaks the mirror symmetry of the spin texture, magnons passing through one undergo a topological spin Hall effect. We have predicted the form of this force in semiclassical transport in Ref. 30; the result is qualitatively similar to the electron case, and involves coupling to the emergent magnetic field of the skyrmion.

Like electrons’ spin degree of freedom, antiferromagnetic spin waves carry a spinor-valued internal degree of freedom called the magnon isospin.<sup>30</sup> It arises due to the two-fold sublattice structure, and characterizes the polarization and handedness of the staggered order precession.<sup>12</sup> Its  $z$ -component on the Bloch sphere is referred to alternatively as the spin wave chirality or the isospin charge, and has shown to be explicitly connected with the breaking of mirror symmetry.<sup>31</sup> This chirality can be associated with magnonic spin currents in easy axis antiferromagnets,<sup>13,30</sup> and tunably generated through spin-transfer torques,<sup>32</sup> circularly polarized light,<sup>33</sup> or oscillating applied magnetic fields.<sup>34</sup>

For antiferromagnetic skyrmions driven by isospin-charged spin waves—that is, those with a circular or elliptical polarization—we expect the mirror symmetry restricting transverse forces to be broken. The consequence, which we show explicitly in the remainder of the

paper, is that the skyrmion experiences transverse forces proportional to the degree of mirror symmetry breaking. And though the anisotropy that associates isospin charge to spin current is necessary to stabilize the skyrmion ground state, we note that the net spin carried by spin waves is immaterial to the skyrmion Hall effect from a symmetry perspective—the handedness of spin wave precession alone is enough to break mirror symmetry across the skyrmion trajectory and induce transverse forces.

Finally, though we are not aware of any prior demonstrations of the effect in the literature, this symmetry argument also suggests that a spin-polarized electron current in an antiferromagnetic metal should produce a skyrmion Hall effect similar to the magnon-driven one we explore in the remainder of this paper. Detailed analysis of this prediction for electronic systems is left to future research.

### III. FORMULATION

In this paper, we work with 2D collinear antiferromagnets with uniaxial anisotropy and broken inversion symmetry. The latter leads to a Dzyaloshinskii-Moriya interaction. In the case of a bipartite,  $g$ -type antiferromagnet, these terms lead collectively to a free energy

$$F = \int [\mathcal{F}_J + \mathcal{F}_D + \mathcal{F}_K] d^2x. \quad (2)$$

Each free energy density is given by

$$\mathcal{F}_J = \frac{Z}{2} \mathbf{m}_A \cdot \mathbf{m}_B - \frac{J}{2} \nabla \mathbf{m}_A \cdot \nabla \mathbf{m}_B, \quad (3a)$$

$$\mathcal{F}_D = \frac{D}{2} [\mathbf{m}_A \cdot (\nabla \times \mathbf{m}_B) + \mathbf{m}_B \cdot (\nabla \times \mathbf{m}_A)], \quad (3b)$$

$$\mathcal{F}_K = -\frac{K}{2} [(\mathbf{m}_A \cdot \hat{z})^2 + (\mathbf{m}_B \cdot \hat{z})^2], \quad (3c)$$

where  $\mathbf{m}_A(\mathbf{r}, t)$  and  $\mathbf{m}_B(\mathbf{r}, t)$  are the continuum representation of the  $A$ - and  $B$ -sublattice magnetic orders. These are normalized vectors, with the saturation magnetization  $M_s$  on each sublattice absorbed into the interaction coefficients. The antiferromagnetic exchange energy  $J$  is that of the underlying lattice Hamiltonian  $\sum_{\langle ij \rangle} J \mathbf{m}_i \cdot \mathbf{m}_j$ , while  $Z$  is the exchange energy density.  $K$  gives the strength of the uniaxial magnetocrystalline anisotropy. We have expressed the Dzyaloshinskii-Moriya interaction with strength  $D$  in the form that arises from bulk inversion symmetry breaking; substituting  $\nabla \mapsto \hat{z} \times \nabla$  in this term recovers the interfacial version of the interaction with no qualitative change in the dynamics.<sup>30</sup>

We will assume that the ground state of the system is collinear and antiferromagnetic, with the ground state  $\mathbf{m}_A^0 = \hat{z}$  and  $\mathbf{m}_B^0 = -\hat{z}$  for concreteness. This constrains the value of  $D$  to lie below the critical value that would lead to a spiral state.<sup>24</sup> We present this model for consistency with other theoretical literature, but our simulation results and many important applications for anti-

ferromagnetic skyrmions take place in synthetic antiferromagnets. Our model also captures these systems with only small quantitative adjustments.<sup>35</sup>

To treat magnon-skyrmion interactions, we implement the formalism laid out in Ref. 30. The magnetization fields  $\mathbf{m}_A$  and  $\mathbf{m}_B$  are decomposed into their fast and slow modes, which represent magnon and skyrmion dynamics, respectively.<sup>5</sup> This separation is valid so long as the spin texture can be modeled as passing through quasistatic equilibria of the magnetic free energy, though at high speeds emergent relativistic effects can become important,<sup>36</sup> which we do not model here. The magnon modes are collected into a 4D vector and obey a Schrödinger-like equation of motion. The spin texture information of the staggered order  $\mathbf{n}(\mathbf{r}) = (\theta(\mathbf{r}), \phi(\mathbf{r}))$  is represented by an emergent magnetic field  $\mathbf{B} = B\hat{z} = \hat{z} \sin\theta(\nabla\theta \times \nabla\phi)$  corresponding to the integrand of Eq. (1).<sup>20</sup> Unlike in Ref. 30, we preserve Lagrangian terms at zeroth order in the spin wave fields, which will give the inertial response of the spin texture. The details of this sector of our Lagrangian are equivalent to the Lagrangian underlying Ref. 37.

### IV. SKYRMION-INDUCED MAGNON HALL EFFECT

In Ref. 30, we have recently worked out the general semiclassical transport theory for antiferromagnetic spin waves in a system such as that defined by Eq. (2). Here we specialize that result to the skyrmion case. Recall that there are two degenerate spin wave modes in the uniform easy-axis antiferromagnet, which correspond to right- and left-handed precessions of the staggered order. A coherent magnonic excitation can be indexed by a spinor quantity  $\boldsymbol{\eta}$  quantifying the linear combination of right- [ $\boldsymbol{\eta} = (1, 0)$ ] and left-handed [ $\boldsymbol{\eta} = (0, 1)$ ] components. We take  $\boldsymbol{\eta}$ , the magnon isospin, to be normalized for a single magnon wave-packet. When the right- and left-handed magnon frequency bands are degenerate,  $\boldsymbol{\eta}$  indexes that degenerate subspace and can explore the Bloch sphere with no energy cost. The addition of the Dzyaloshinskii-Moriya interaction breaks this degeneracy, but only weakly, so certain rotations of  $\boldsymbol{\eta}$  incur small energy costs.<sup>38,39</sup>

We will assume that the skyrmion in our problem is rigid—that is, its shape is fixed but its position may vary. This assumption implies that time dependence of the spin texture can be factored through the rigid skyrmion's position coordinate  $\mathbf{R} = (X(t), Y(t))$ . The semiclassical Lagrangian for a single magnon wave-packet is given by

$$L_{\text{WP}} = -\boldsymbol{\eta}^\dagger \left[ \sigma_z (\dot{\mathbf{A}} \cdot \mathbf{r} - V) - \dot{\mathbf{k}} \cdot \mathbf{r} - \mathcal{H} \right] \boldsymbol{\eta}, \quad (4)$$

with  $\mathbf{r}$  and  $\mathbf{k}$  the wave-packet's phase space variables,  $\sigma_z$  the usual Pauli matrix, and  $\mathbf{A}(\mathbf{r}, t)$  and  $V(\mathbf{r}, t)$  vector and scalar potential functions underlying the emergent electromagnetic fields.<sup>20,40,41</sup> The vector potential is related to the skyrmion's emergent magnetic field through

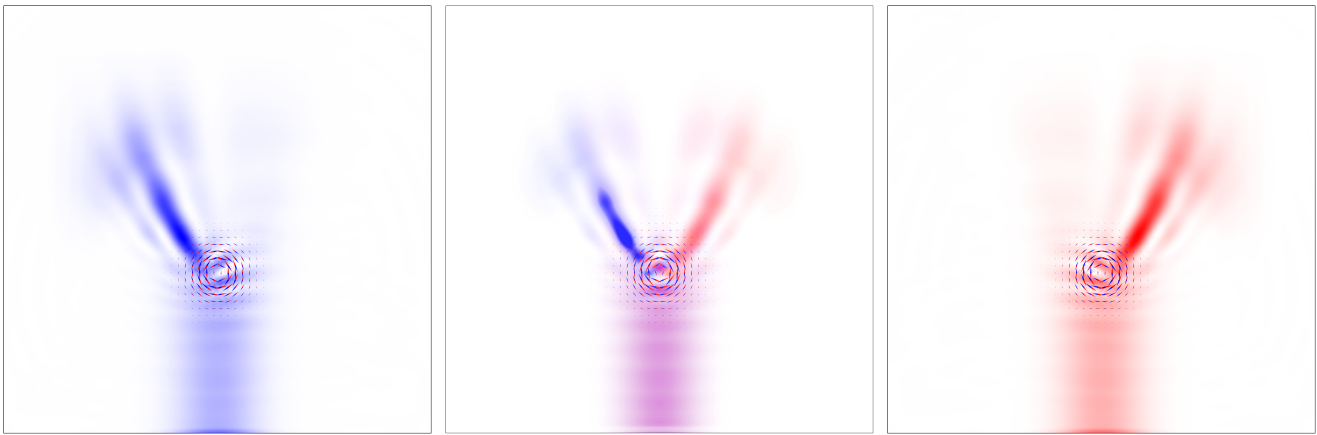


FIG. 2. Micromagnetic simulations of the magnonic topological spin Hall effect in antiferromagnetic skyrmions. Blue and red represent left and right handed spin wave precession of the local Néel order about equilibrium, plotted as the square of the spin wave amplitude integrated over the entire simulation time. In all cases, a fluctuating magnetic field injects coherent spin waves ( $\omega/2\pi = 30$  GHz) at the bottom of the frame. Left: left-handed spin waves are deflected to the left. Right: right-handed spin waves are deflected to the right. Center: linearly polarized spin waves, an equal superposition of the left- and right-handed magnon bands, are decomposed by the skyrmion into its spin polarized eigenmodes. The sample size is  $800 \text{ nm} \times 800 \text{ nm}$ .

$\mathbf{B} = \nabla \times \mathbf{A}$ . The  $2 \times 2$  isospin Hamiltonian  $\mathcal{H}$  is derived by projecting out the negative frequency subspace of the  $4 \times 4$  spin wave Hamiltonian governing the  $\hat{\theta}$  and  $\hat{\phi}$  components of  $\mathbf{m}_A$  and  $\mathbf{m}_B$ .<sup>30</sup> With the time dependence of the electromagnetic potentials replaced with the collective coordinate dynamics of  $\mathbf{R}$ , the equations of motion for the magnon wavepackets become

$$\dot{\mathbf{k}} = \chi(\dot{\mathbf{r}} - \dot{\mathbf{R}}) \times \mathbf{B} - \frac{\partial \omega}{\partial \mathbf{r}}, \quad (5a)$$

$$\dot{\mathbf{r}} = \frac{\partial \omega}{\partial \mathbf{k}}, \quad (5b)$$

$$\text{and } i\dot{\boldsymbol{\eta}} = \mathcal{H}\boldsymbol{\eta}, \quad (5c)$$

at second order in derivatives of the spin texture.<sup>42</sup> Here  $\omega = \omega(\mathbf{r})$  is the spin wave frequency of the local magnon band structure and  $\chi = \boldsymbol{\eta}^\dagger \sigma_z \boldsymbol{\eta}$  is the emergent charge.

The isospin charge  $\chi$  corresponds to the handedness of the spin wave: it is  $\pm 1$  for right- and left-handed waves, and vanishes for linearly polarized waves. That it acts as the coupling constant between magnon and skyrmion reflects our symmetry arguments from Sec. II: the degree and sign of mirror symmetry breaking controls the transverse force on the magnon. We expect from Eq. (5a) that right- and left-handed waves experience oppositely signed Lorentz forces in the presence of a skyrmion spin texture.

To verify this prediction, we carried out micromagnetic simulations of a skyrmion in a synthetic antiferromagnet. We numerically solved the Landau-Lifshitz-Gilbert equation using finite elements methods code.<sup>43-46</sup> The parameters are chosen following Refs. 44 and 47: gyromagnetic ratio  $\gamma = 2.21 \times 10^5 \text{ Hz}/(\text{A}/\text{m})$ , exchange stiffness  $\mathcal{J} = 4.00 \times 10^{-12} \text{ J}/\text{m}$ , Dzyaloshinskii-Moriya energy  $\mathcal{D} = 1.23 \times 10^{-4} \text{ J}/\text{m}^2$ , anisotropy energy  $\mathcal{K} = 4.73 \times 10^3 \text{ J}/\text{m}^3$ , and interlayer antiferromagnetic energy

$\mathcal{Z} = 6.09 \times 10^4 \text{ J}/\text{m}^3$ . We set the Gilbert damping to  $\alpha = 10^{-4}$ . In these simulations, we generated either circularly polarized spin waves, by applying a rotating magnetic field  $\mathbf{h}_{\text{RH/LH}} = h_0 [\sin(\omega t)\hat{x} \mp \cos(\omega t)\hat{y}]$ , or linearly polarized spin waves, by applying  $\mathbf{h}_X = h_0 \sin \omega t \hat{y}$  or  $\mathbf{h}_Y = h_0 \sin \omega t \hat{x}$  for X- or Y-polarizations.

The results are displayed in Fig. 2. We find that scattering right-handed ( $\chi = +1$ ) and left-handed ( $\chi = -1$ ) spin waves from the skyrmion results in right-ward and left-ward deflection, respectively. Leftward deflection of right-handed magnons from a skyrmion is consistent with the ferromagnetic skyrmion Hall effect;<sup>6,7</sup> as left-handed magnons do not exist in ferromagnets,<sup>48</sup> we find that this latter effect is a uniquely antiferromagnetic phenomenon. When linearly polarized spin waves ( $\chi = 0$ ) are injected upon the skyrmion texture, the skyrmion splits the signal into its two spin polarized channels, producing a transverse spin current with no net transverse magnon number current. This result for linearly polarized waves is analogous from a symmetry perspective to the electronic topological spin Hall effect predicted in Ref. 26.

While the spin waves are strongly deflected by the Lorentz force in Eq. (5a), their isospin degree of freedom does not remain static throughout this process. According to Eq. (5c), the isospin vector itself undergoes dynamics in the presence of a nontrivial  $\mathcal{H}$ , such as arises within the skyrmion texture. This in turn affects the isospin charge  $\chi$ . Even supposing that a purely right-handed spin wave signal enters the skyrmion, it will constantly undergo some isospin dynamics, resulting in the production of some signal in the left-handed channel. Consequently, the nearly right-hand polarized signal exiting the skyrmion picks up some ellipticity in Fig. 2. Though our simulations show signs of this behavior, the effect is small; it is also difficult to isolate, occurring mainly near

the skyrmion core. Attempting to incorporate these dynamics into the equation for the Lorentz force indicates an angular momentum transfer between magnon isospin and mechanical angular momentum of the skyrmion, but only at higher orders in perturbation theory than Eqs. (5) can express. We expect that any effect on the dynamics of magnon and skyrmion trajectories is negligible.

Since antiferromagnetic skyrmions present a real-space Berry curvature, magnons act as charged particles in the presence of a perpendicular magnetic field. In a finite geometry, one might therefore expect chiral edge modes in an antiferromagnetic skyrmion crystal. Using micromagnetic simulations, we injected right- and left-handed spin waves into a nanodisk with an artificially constructed antiferromagnetic skyrmion lattice. The results are shown in Fig. 3. Modes propagate away from the antenna in the direction according to their handedness, decaying naturally via Gilbert damping. A more quantitative analysis of this result has recently been developed from lattice-level transport theory.<sup>49</sup>

## V. SKYRMION COLLECTIVE COORDINATE THEORY

The spin wave dynamics and magnon-skyrmion interactions summarized in the previous section are captured at the semiclassical level by a wave-packet Lagrangian  $L_{WP}$  that leads to Eqs. (5).<sup>30</sup> A Lagrangian for the full system can be obtained by adding to  $L_{WP}$  a sector detailing the inertial properties of the skyrmion.

Write the density of magnons at  $(\mathbf{r}, \mathbf{k})$  in phase space, with isospin  $\boldsymbol{\eta}$ , as  $\rho_{\mathbf{r},\mathbf{k},\boldsymbol{\eta}}$ . Accepting an uncertainty  $\Delta\mathbf{r}\Delta\mathbf{k} \geq 2\pi$ , we can expand the global wavefunction of magnons into a linear combination of wavepackets. The total Lagrangian for all the wavepackets together is merely their weighted sum

$$L_{SWs}[\rho; \mathbf{B}] = \int d^2\mathbf{r} d^2\mathbf{k} d^2\boldsymbol{\eta} \rho_{\mathbf{r},\mathbf{k},\boldsymbol{\eta}} L_{WP}[\mathbf{r}, \mathbf{k}, \boldsymbol{\eta}, \mathbf{B}]. \quad (6)$$

The uncertainty principle constraining this expansion means that the following predictions will hold best for skyrmions large and smooth compared to magnon wavelength. From Eq. (6) we can immediately take a functional derivative with respect to  $\mathbf{R}(t)$  to obtain the magnonic force density over phase space. The result is

$$\frac{\delta L_{WP}}{\delta \mathbf{R}} = -\rho_{\mathbf{r},\mathbf{k},\chi} \chi (\dot{\mathbf{r}} - \dot{\mathbf{R}}) \times \mathbf{B}_0(\mathbf{r} - \mathbf{R}) \quad (7)$$

where  $\mathbf{B}_0(\mathbf{r} - \mathbf{R}) = \mathbf{B}(\mathbf{r})$ . The total magnonic force on the skyrmion is therefore

$$\mathbf{F} = - \int d^2\mathbf{r} d^2\mathbf{k} d^2\boldsymbol{\eta} \chi \rho_{\mathbf{r},\mathbf{k},\chi} \left[ (\dot{\mathbf{r}} - \dot{\mathbf{X}}) \times \mathbf{B}_0(\mathbf{r} - \mathbf{R}) \right], \quad (8)$$

an isospin-charge-weighted sum of the reciprocal Lorentz forces by each magnon. Since  $\mathbf{B}_0$  is radially symmetric, the component of  $\mathbf{F}$  perpendicular to the current flow

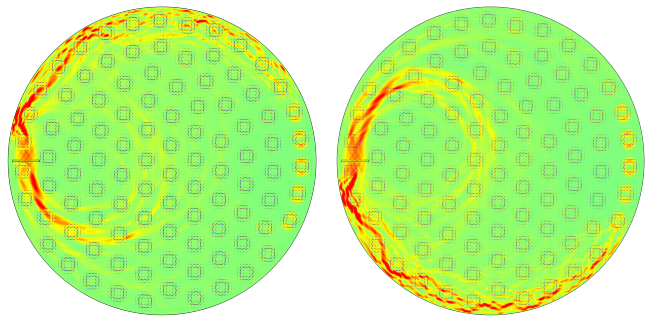


FIG. 3. Edge modes of the antiferromagnetic skyrmion crystal. The color scale gives the squared spin wave amplitude integrated over the full simulation time. A simulated microwave antenna sits above the nanodisk on left side of the sample, indicated by a horizontal line. Left and right-handed spin waves are injected at 20 GHz in figures left and right, respectively. As in the common toy model of the quantum spin Hall effect, cyclotron orbits of the magnons combined with an effective confining potential at the edge restrict the magnon trajectories to chiral directions corresponding to their isospin. The sample diameter is 1300 nm, and the snapshot was taken 2.1 ns into the simulation. Gilbert damping causes the spin wave intensity to decay away from the antenna.

$\mathbf{j} \propto \langle \dot{\mathbf{r}} \rangle$  will vanish only if the isospin charge distribution  $\chi \rho_{\mathbf{x},\mathbf{k},\boldsymbol{\eta}}$  happens to be asymmetric across  $\mathbf{j}$ . A special case of this condition occurs when the incoming current is entirely unpolarized, as in the center panel of Fig. 2, analogous to the electronic case discussed widely in the literature and noted in Sec. II.

Outside of this special case, the transverse force component has considerable freedom. In Fig. 4 we show micromagnetic simulation results of antiferromagnetic skyrmion trajectories driven by right, left, and linearly polarized spin waves. There are two crucial differences from the ferromagnetic case. First, the angle at which the skyrmion propagates can be tuned by tuning the chirality of the driving magnon current. Second, because the Lorentz force is the only force term present, and because antiferromagnetic skyrmions have primarily diagonal mass tensors, antiferromagnetic skyrmions move along, rather than against, the magnon current driving them. The opposite is known to happen in ferromagnetic skyrmion systems,<sup>5</sup> which we replicate in Fig. 4 by turning off the interlayer coupling of our synthetic antiferromagnetic and allowing the two sublattice skyrmions to behave as ferromagnetic skyrmions would. Their reversed solutions are indicated in the figure by black trajectories.

### A. Magnon-mediated reduction in effective mass

The qualitative inertial behavior of antiferromagnetic skyrmions is well-studied in the literature,<sup>37</sup> so we do not dwell on a detailed derivation here. As a rule and in the rigid skyrmion approximation, antiferromagnetic

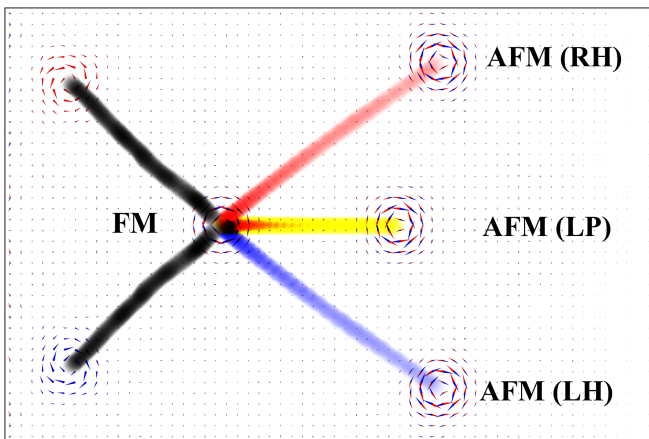


FIG. 4. Overlaid skyrmion trajectories of multiple simulations in a  $1200\text{ nm} \times 800\text{ nm}$  system. In all cases, a spin wave current with wavenumber  $k = 0.063\text{ nm}^{-1}$  flows from left to right. The three trajectories on the right correspond to nonzero interlayer coupling  $J_{\text{AF}} \neq 0$ , that is, a synthetic antiferromagnet. These trajectories are plotted at a snapshot time of 2.3 ns, and here  $\omega(k) = 15.7\text{ GHz}$ . Yellow: an antiferromagnetic skyrmion is driven longitudinally, with no net Magnus force, by linearly polarized spin waves. Blue: an antiferromagnet skyrmion is driven to the right by left-handed spin waves. Red: an antiferromagnetic skyrmion is driven to the left by right-handed spin waves. The two black trajectories on the left correspond to  $J_{\text{AF}} = 0$ , giving two decoupled ferromagnets. Here, the sublattice skyrmions move transversely and counter-longitudinally to the magnon current, and the simulation required 100 ns to reach this snapshot. In the ferromagnetic system,  $\omega(k) = 6\text{ GHz}$ .

skyrmions behave as classical Newtonian point particles, complete with a mass term with its origins in the sublattice interaction and the small magnetic moment carried by the skyrmion. The non-interacting part of the skyrmion Lagrangian is just

$$\mathcal{L}[\mathbf{R}](\mathbf{r}, \mathbf{k}) = \frac{1}{2} \tilde{m}_{ij} \dot{R}_i \dot{R}_j - \frac{S}{2} \omega \rho_n \epsilon^2 \quad (9)$$

with the magnon number density  $\rho_n = \int d^2 \eta \rho_{\mathbf{r}, \mathbf{k}, \eta}$ , the emergent skyrmion mass density tensor  $\tilde{m}_{ij}(\mathbf{r}, \mathbf{k}) = (S/\Omega)[2^{-1/2} - \rho_n(\mathbf{r}, \mathbf{k})\omega(\mathbf{r}, \mathbf{k})/\Omega]g_{ij}(\mathbf{r})$ , with the characteristic frequency of the exchange interaction  $\Omega = Z\epsilon^2/S$ , and  $\epsilon$  the lattice constant. We presume a square lattice for concreteness. The induced metric tensor  $g_{ij}$  on spin space is defined as  $g_{ij} = \partial_i \theta \partial_j \theta + \sin^2 \theta \partial_i \phi \partial_j \phi$ .

The second term on the right-hand side of Eq. (9) is a potential energy landscape presented to the skyrmion by the global magnon wavefunction. Though we have claimed that this is the “non-interacting” part of the Lagrangian, the presence of spin waves in the system softens the order parameter of the skyrmion. This suggests that a skyrmion left to its own devices would flow toward regions of high magnon density; this matches with recent results indicating that antiferromagnetic skyrmions will flow along the direction of a thermal gradient,<sup>27,50</sup> though

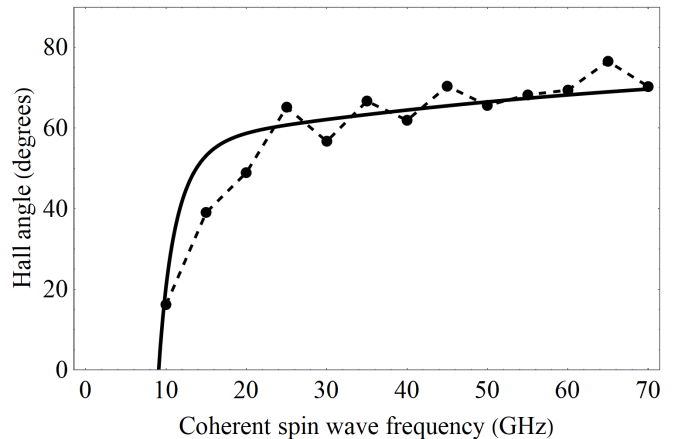


FIG. 5. Simulation and theory results for the skyrmion Hall angle driven by chirally polarized spin waves. Dashed lines connect the data from micromagnetic simulation; the solid line gives the theoretical prediction according to Eq. (10). Skyrmion position was tracked by a position-weighted expectation value of the skyrmion charge density, that is, Eq. (1) taken with a factor of  $\mathbf{x}$  in the integrand.

this could also be attributed to the direct magnon forces in the interacting Lagrangian.

The first term on the right-hand side of Eq. (9) is the skyrmion’s kinetic energy term. The mass tensor of antiferromagnetic textures in the absence of spin wave excitations has been derived previously by Tveten *et al.* in Ref. 37. Our solution agrees<sup>51</sup> with theirs when the magnon number density vanishes,  $\rho_n = 0$ . When  $\rho_n \neq 0$ , the form of the mass tensor in Eq. (9) indicates that the presence of spin waves in a skyrmion (or any other spin texture described by rigid coordinates) will lower the skyrmion’s effective mass.

This mass reduction scales with the number and frequency of spin waves, that is, with the total spin wave energy present in the skyrmion. We predict that this reduction should occur in any antiferromagnetic skyrmion system, including those driven by electric current, as skyrmion motion itself produces spin waves. This mass reduction suggests skyrmion mobility should be increased in higher temperature systems, where thermal magnon populations exist throughout the system. This is consistent with findings in the literature<sup>8,50</sup> that the diffusion constant for an antiferromagnetic skyrmion increases with temperature, though any precise discussion of the relationship between magnon-driven mass reduction and diffusive behavior, along with the relative contributions of the mass reduction and the static potential term on the far right of Eq. (9) is left to future research.

## B. Frequency-dependent kinematics

We have seen that the sign and amplitude of the skyrmion Hall angle is tunable by changing the chirality

of the driving magnon current. Although ferromagnetic skyrmion systems cannot change the sign of this angle, the amplitude is known to depend on the frequency of the driving spin waves.<sup>6,7</sup> In these systems, the Hall angle increases monotonically with spin wave frequency until reaching a critical frequency, past which the Hall angle decays to zero as frequency continues to increase. We have indicated this ferromagnetic behavior schematically with the dashed line in Fig. 5.

We investigated the frequency dependence of the skyrmion Hall angle in simulation, and present our results in Fig. 5. These results (solid line and points) indicate a strong dissimilarity to the ferromagnetic behavior at high frequencies. The lack of a critical frequency for optimal Hall deflection is an attractive property for skyrmionic devices, as one can achieve uniform angular propulsion without the need to fine tune the driving frequencies.

The origin of this divergence from the ferromagnetic physics lies, essentially, in the magnon dispersion relation. As the frequency of a ferromagnetic spin wave increases, so does its group velocity. Modeling its interaction with the skyrmion as that of a charged particle passing through a region of magnetic flux, we can understand the high frequency decay of the ferromagnetic skyrmion Hall angle as an explosion of the magnon cyclotron radius at high velocity.<sup>6</sup>

In antiferromagnetic systems, the well-known linear dispersion<sup>52</sup> at high wavenumber ensures that, away from the band bottom, group velocity does *not* increase with increasing frequency. As we move away from the band bottom where anisotropy induces a locally parabolic dispersion, the group velocity of the magnon saturates, and so the magnon cyclotron radius and corresponding skyrmion Hall angle do as well.

### C. Flux disk model

To model the frequency dependence using our theoretical framework, we adopt the simplifying assumption that the skyrmion can be modeled as a disk of uniform flux. The  $4\pi Q$  emergent magnetic flux that a real skyrmion would distribute according to the profile of  $\mathbf{B}$  is instead distributed uniformly over a disk of radius  $R$ , the skyrmion radius. This approximation has been used in past analyses of magnon-skyrmion scattering with great success.<sup>6</sup>

Further assuming that the magnitude of the group velocity does not change over the course of its passage through the skyrmion, the magnon scattering problem reduces to understanding the intersection of two circles: the skyrmion circumference and the cyclotron orbit of the magnon wavepacket, which we define to have radius  $r$ . We then wish to analyze the change in direction accumulated by a magnon entering the skyrmion from the  $-\hat{y}$  direction. The problem enjoys a helpful constraint: the center of the cyclotron orbit has the same  $y$  coordinate as the point of entry  $(x, y)$  to the flux disk. It

is an exercise in planar geometry to then show that the angle subtended by the cyclotron orbit restricted to the flux disk is given by  $\sin(\theta/2) = \sqrt{1 - \xi^2}/\sqrt{1 + \rho^2 + 2\rho\xi}$ , where  $\rho = r/R$  and  $\xi = x/R$ . The angle between the  $\Delta\hat{\mathbf{x}}$  induced by this cyclotron motion and the  $\hat{y}$  axis is just  $\Theta_{SH} = (\pi - \theta)/2$ , which will also be the skyrmion Hall angle by momentum conservation.

The problem of determining a closed expression for the skyrmion Hall angle therefore reduces to finding the normalized cyclotron radius  $\rho(\xi)$ . Choosing the Lorentz force as our lone centripetal force, we have  $\rho = mvR/4\chi Q$  where we have set the magnetic flux density to  $B = 4\pi Q/R^2$ . Now, supposing that the incoming magnon current is distributed uniformly along the  $\hat{x}$  direction, the mean outgoing angle is

$$\langle\theta\rangle = \frac{1}{2} \int_{-1}^1 \theta(\xi) d\xi = \frac{\pi}{2\rho} = \frac{2\pi\chi Q}{mvR}, \quad (10)$$

which formally converges only in the case  $\rho > 1$ . Finally, from Eqs. (5), extract speed  $v = |\partial\omega/\partial\mathbf{k}|$  and effective mass  $m = 1/|\partial^2\omega/\partial\mathbf{k}^2|$ . Using the spin wave dispersion outside the skyrmion,

$$\omega = \sqrt{(Jk^2 + Dk + K)(Jk^2 + Dk + K + Z)}, \quad (11)$$

we plot the Hall angle prediction given by Eq. (10) in Fig. 5.

The remarkable agreement between this simple model and micromagnetic simulation suggests that the purely electrodynamic modeling of the magnon-skyrmion interaction captures most of the important Hall effect physics. The magnon wavelength ranges from roughly 200 nm at the lowest frequency to roughly 30 nm at the highest frequency, which is on the order of the skyrmion radius.

In Fig. 6, we plot the skyrmion speed as a function of driving frequency. At reasonable frequencies, the skyrmion reaches speeds on the order of 100 m/s, comparable with fast electron-driven ferromagnetic skyrmions. These speeds are also comparable to those predicted for antiferromagnetic skyrmions driven by a thermal gradient.<sup>53</sup> In the same system with the same parameters, driving our skyrmion with a current-induced spin-transfer torque gave speeds on the order of 1000 m/s, consistent with the literature.<sup>17</sup> Though the magnonic drive cannot reach the speeds of an electronic drive in antiferromagnets, it readily competes with high speed ferromagnetic systems and could provide a feasible low-energy route to antiferromagnetic skyrmionics.

That the linearly polarized modes produce a slower speed can be partially attributed to the competition between right- and left-handed waves. In the circular spin wave case, the change of momentum for each spin wave component is unimodal and strongly concentrated around that mode, as in the left and right panes of Fig. 2. The momentum transferred to the skyrmion will be proportional to the total  $\Delta\mathbf{k}$  vector lost by these spin waves, which will be proportional to  $2\Theta_{SH} - \pi$ .

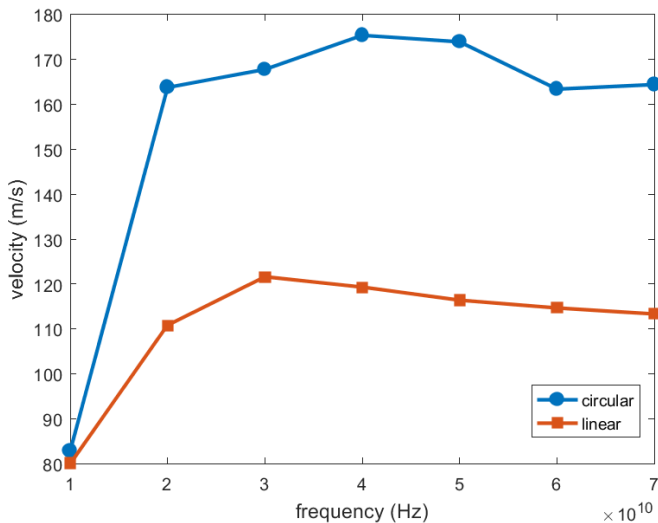


FIG. 6. Skymion velocity as driven by coherent spin wave signals, of either circular or linear polarization, driven by circularly or linearly polarized magnetic fields of equal amplitude. The plotted frequency range corresponds to the same dynamical range above the resonant frequency as in Fig. 5. Skymion position was tracked by a position-weighted expectation value of the skymion charge density, that is, Eq. (1) taken with a factor of  $\mathbf{x}$  in the integrand.

In the linearly polarized case, depicted in the central pane of Fig. 2, horizontal components of the magnonic force on the skymion cancel each other. As we discussed at length in the beginning of the manuscript, this cancellation provides for the observed absence of a skymion Hall effect in many previous investigations of antiferromagnetic skymion dynamics. This is a preferable quality of many skymion based devices, but we see here that it comes at a cost. The cancellation of these opposite spin Hall channels also wastes some of the momentum transfer from magnon to skymion.

If this Lorentz force were the lone mechanism responsible for this behavior, then we would expect  $v_L = v_C \cos(2\Theta_{SH})$ , where  $v_L$  and  $v_C$  are the velocities under linear or circular spin wave drive. That is to say, we expect the transverse component to be the same in each case, with the linear drive losing speed only by virtue of lacking a transverse component. This relation describes the relationships of Fig. 6 well at high frequencies, but does very poorly at low frequencies. This seems to suggest that at low frequencies, where the spin wave wavelength is much bigger than the skymion radius, a significant failure mode arises in the simple analysis we have given above.

The primary failure mode of our analysis as applied to the skymion velocity lies in the fact that we have neglected the conservative force  $-\partial\omega/\partial\mathbf{r}$  in Eq. (5). Though at high frequencies this force will differ between circularly and linearly polarized currents only perturbatively at  $O(D)$ , we expect this missing force to be significantly ( $O(1)$ ) polarization-dependent at low frequencies.

Studies on antiferromagnetic domain walls have shown that the transmission spectra of alternately polarized antiferromagnetic spin waves vary significantly below a critical frequency determined by the Dzyaloshinskii-Moriya interaction and uniaxial anisotropy at the center of the domain wall.<sup>43</sup> Understanding the low frequency regime therefore requires a truly wave-theoretic analysis; our wavepacket quasiparticles are not sensible constructions when they are subject to partial transmission and reflection.

As a result of nontrivial transmission and reflection, spin waves at sufficiently lower energy may also become trapped inside the energy barrier along the skymion's circumference, filling bound magnon states of the skymion texture. We are not aware of any thorough investigations of these bound states in antiferromagnets, but they are known to cause significant modifications in the physics of ferromagnetic skymions.<sup>7</sup> We have alluded to some of the effects such states may have in antiferromagnetic skymions, such as the mass reduction explored in Sec. V A, but a thorough study of these phenomena is beyond the scope of the manuscript. We expect future research in this area could be extremely interesting, and may differ significantly from the ferromagnetic physics, for two key reasons. First, unlike in ferromagnets, the spin carried by the bound magnon states is not locked to the background texture. Second, the dynamics of the spin carried by these bound modes could be very rich; a bound mode initially occupied by an externally driven right-handed magnon can undergo a dynamical evolution of its isospin,<sup>30</sup> and the full effects of such an evolution are yet unknown. In general, the spectrum of bound modes and corresponding vibrational modes of the skymion are complicated questions, and only recently are full classifications of these degrees of freedom beginning to be fully explored in general solitonic systems.<sup>54</sup>

## VI. APPLICATIONS

The previous sections have laid out theory and simulations of the skymion and topological spin Hall effects in antiferromagnets. In the present section, we discuss how these phenomena might be put to use as components in a magnonic or skymionic logic device.

Ideas around magnonic logic have been around for some time<sup>55</sup> and are traditionally considered for implementation in ferromagnets. Though comparatively young, the enterprise of antiferromagnetic magnonics has potential advantages. It has been pointed out by many authors that antiferromagnetic insulators lack stray fields and would avoid cross-talk between tightly packed devices. The terahertz regime in which antiferromagnetic dynamics operates is widely regarded as attractive for its speed and its uniqueness among solid state systems, which generally operate in lower frequency bands.

Another limitation of ferromagnetic magnonics is that it can use only amplitude and phase to encode informa-

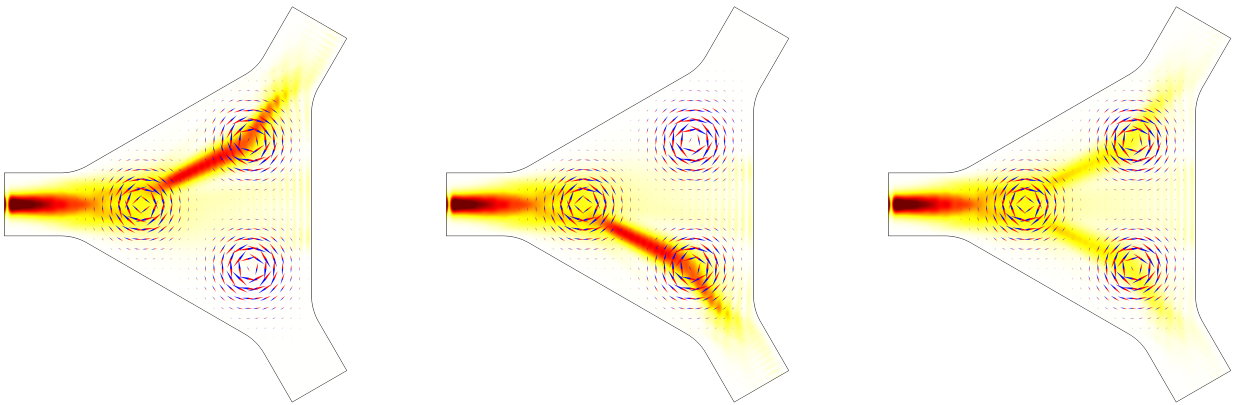


FIG. 7. Spin wave circulators implemented using antiferromagnetic skyrmions. In all cases, a spin wave current is injected from the left. Spin polarized magnon currents circulate about the device with the handedness of their internal isospin. For linearly polarized waves, the circulator acts as an isolator/filter for the spin eigenmodes. The radius from device center to the central edge of any port is 200 nm; the injected spin waves have frequency 0.2 THz. The color scale represents the square of the spin wave amplitude integrated over the full simulation time.

tion, as these are the only dynamical degrees of freedom available. Antiferromagnets possess an additional degree of freedom, the isospin, whose interaction with skyrmions this manuscript has addressed. Whereas ferromagnetic spin waves are bound by the background magnetization texture to carry a particular spin current, antiferromagnetic spin waves are not. Naturally, this increases the amount of information they can carry. It also changes the nature of the computation, because the order of operations on an antiferromagnetic spin wave signal affects the outcome<sup>30</sup>. Lebrun et al. have recently pointed out that the isospin degree of freedom can also allow us to distinguish coherent magnon signals from thermal magnon currents, which will be spin unpolarized in general.<sup>50,56</sup> In ferromagnets, of course, thermal magnons carry the same sign of spin as coherent magnons.

Because skyrmions couple differently to spin up and spin down magnonic currents, they could be used in principle as part of a magnonic logic device. We outlined in Ref. 30 how inversion symmetry breaking, domain walls, and other components of the antiferromagnetic free energy could be used to realize unitary rotations of the isospin vectors  $\eta$ . The use of a skyrmion-induced topological spin Hall effect, however, would be quite different. Since the skyrmion projects a signal into its spin channels, it acts explicitly as a nonlinear element that cannot be captured as a unitary transformation. As such, it is also nonreciprocal: sending an output spin wave back into the skyrmion does not direct it toward the original input. This notion is exemplified by a device called a spin wave circulator.

The circulator, more generally, is a nonreciprocal device which can separate input and output channels. It has been widely used to realize full-duplex communication in nonmagnonic media: the microwave circulator<sup>57</sup> and acoustic circulator<sup>58</sup> are two examples. Spin-wave circu-

lators are expected to be critical components of magnonic computers.<sup>59</sup> Using the topological spin Hall effects outlined in this article, we present the design of a spin-wave circulator based on skyrmions in a synthetic antiferromagnet in Fig. 7, where three skyrmions are confined in a three-terminal structure.

Due to the skyrmion-skyrmion and the skyrmion-edge repulsion, the skyrmions are stable in such a structure as shown in the micromagnetic simulation results of Fig. 7. The three ports of the circulator are structurally equivalent. The spin channel projection behavior is shown in Fig. 7. Incoming magnons are successively scattered by two skyrmions to either the top or bottom output ports, depending on their spin. Mixed signals are split into their two spin components.

## VII. CONCLUSION

In this article, we explored the Hall effects arising from magnon-skyrmion interactions in easy-axis antiferromagnetic insulators. The underlying principle for these effects is the breaking of mirror plane symmetry across quasiparticle trajectories: in the magnon case, broken by the skyrmion spin texture; and in the skyrmion case, broken dynamically by the unbalanced scattering profile of a circularly polarized magnon current. Unlike the ferromagnetic case (where the sign of the skyrmion Hall angle cannot be tuned), antiferromagnetic skyrmions offer a large range of dynamic tunability that could be put to use in logical or neuromorphic magnonic systems.

We have explored the magnonic case here, where chiral spin waves could in principle be generated electronically, optically, or thermally. However, even spin polarized electron currents can be produced in antiferromagnetic metals,<sup>60,61</sup> giving unbalanced spin transfer torques

on the sublattices and breaking the mirror symmetry we discussed in Sec. II to produce Hall physics. Even when the skyrmion does not move, the spin Hall effect it produces could be useful in such computing schemes, or as an experimental method for inferring a skyrmion's existence.

We emphasize that although our micromagnetic simulations focused on synthetic antiferromagnets, our theory is equally applicable to both synthetic and traditional, bipartite antiferromagnets. Whereas the former are easily probed in experiment, observing skyrmion-scale spin textures in antiferromagnets can be a challenge. Using spin Hall signals as an indirect means of observation may be a useful tool both experimentally and in skyrmion-based devices. The parameters we used in our micromagnetic simulations correspond approximately to two antiferromagnetically coupled layers of yttrium iron garnet (YIG), as have been used in a variety of similar studies.<sup>44,47</sup> Recently, experimental work has demonstrated antiferromagnetic coupling between ultrathin bilayers of yttrium

iron garnet and gadolinium iron garnet (GdIG).<sup>62</sup> This realization of an insulating, two-dimensional synthetic antiferromagnet would be an ideal system for testing the topological spin Hall effect we described in this paper.

M.W.D. and W.Y. contributed equally to this work. We would like to thank Xiaochuan Wu, Jin Lan, and Mark D. Stiles for insightful discussions. This work was supported by the Cooperative Research Agreement between the University of Maryland and the National Institute for Standards and Technology, award 70NANB14H209, through the University of Maryland (M.W.D.), the NSF East Asia and Pacific Summer Institute under award number EAPSI-1515121 (M.W.D.), the China Postdoctoral Science Foundation, project number 2018M641906 (W.Y.), the National Natural Science Foundation of China project number 11847202 (W.Y.), the National Natural Science Foundation of China grant number 11722430 (J.X.), and the Defense Advanced Research Project Agency (DARPA) program on Topological Excitations in Electronics (TEE) under grant number D18AP00011 (D.X.).

- 
- \* Corresponding author: matthew.daniels@nist.gov
- <sup>1</sup> A. Belavin and A. Polyakov, J. Exp. Theor. Phys. Lett. **22**, 245 (1975).
  - <sup>2</sup> A. A. Thiele, Phys. Rev. Lett. **30**, 230 (1973).
  - <sup>3</sup> M. Stone, Phys. Rev. B **53**, 16573 (1996).
  - <sup>4</sup> O. Tchernyshyov, Ann. Phys. **363**, 98 (2015).
  - <sup>5</sup> L. Kong and J. Zang, Phys. Rev. Lett. **111**, 067203 (2013).
  - <sup>6</sup> J. Iwasaki, A. J. Beekman, and N. Nagaosa, Phys. Rev. B **89**, 064412 (2014).
  - <sup>7</sup> C. Schütte and M. Garst, Phys. Rev. B **90**, 094423 (2014).
  - <sup>8</sup> J. Barker and O. A. Tretiakov, Phys. Rev. Lett. **116**, 147203 (2016).
  - <sup>9</sup> X. Zhang, Y. Zhou, and M. Ezawa, Sci. Rep. **6**, 24795 (2016).
  - <sup>10</sup> C. Jin, C. Song, J. Wang, and Q. Liu, Appl. Phys. Lett. **109**, 182404 (2016).
  - <sup>11</sup> X. Zhang, M. Ezawa, and Y. Zhou, Phys. Rev. B **94**, 064406 (2016).
  - <sup>12</sup> F. Keffer and C. Kittel, Phys. Rev. **85**, 329 (1952).
  - <sup>13</sup> R. Cheng, J. Xiao, Q. Niu, and A. Brataas, Phys. Rev. Lett. **113**, 057601 (2014).
  - <sup>14</sup> S. Seki, T. Ideue, M. Kubota, Y. Kozuka, R. Takagi, M. Nakamura, Y. Kaneko, M. Kawasaki, and Y. Tokura, Phys. Rev. Lett. **115**, 266601 (2015).
  - <sup>15</sup> Y. Shiomi, R. Takashima, and E. Saitoh, Phys. Rev. B **96**, 134425 (2017).
  - <sup>16</sup> H. Velkov, O. Gomonay, M. Beens, G. Schwiete, A. Brataas, J. Sinova, and R. A. Duine, New J. Phys. **18**, 075016 (2016).
  - <sup>17</sup> X. Zhang, Y. Zhou, and M. Ezawa, Nat. Comm. **7**, 10293 (2016).
  - <sup>18</sup> The order parameter is embedded in 3D, but in principle it must have unit magnitude or nearly unit magnitude to give sensible results.
  - <sup>19</sup> N. Manton and P. Sutcliffe, "Topological Solitons (Cambridge Monographs on Mathematical Physics)," (2004).
  - <sup>20</sup> N. Nagaosa and Y. Tokura, Nat. Nano. **8**, 899 (2013).
  - <sup>21</sup> H. Velkov, O. Gomonay, M. Beens, G. Schwiete, A. Brataas, J. Sinova, and R. A. Duine, New J. Phys. **18**, 075016 (2016).
  - <sup>22</sup> T. Moriya, Phys. Rev. **120**, 91 (1960).
  - <sup>23</sup> S. Rohart, J. Miltat, and A. Thiaville, Phys. Rev. B **93**, 214412 (2016).
  - <sup>24</sup> S. Rohart and A. Thiaville, Phys. Rev. B **88**, 184422 (2013).
  - <sup>25</sup> R. Cheng and Q. Niu, Phys. Rev. B **86**, 245118 (2012).
  - <sup>26</sup> P. M. Buhl, F. Freimuth, S. Blügel, and Y. Mokrousov, Phys. Status Solidi Rapid Res. Lett. **11**, 1700007 (2017), 1700007.
  - <sup>27</sup> S. K. Kim, K. Nakata, D. Loss, and Y. Tserkovnyak, Phys. Rev. Lett. **122**, 057204 (2019).
  - <sup>28</sup> By *spin unpolarized*, we mean simply that the spin current operator can be factored into its spin and velocity components. A current where both spin channels have the same number current distribution is spin unpolarized by our definition.
  - <sup>29</sup> J. Shi, P. Zhang, D. Xiao, and Q. Niu, Phys. Rev. Lett. **96**, 076604 (2006).
  - <sup>30</sup> M. W. Daniels, R. Cheng, W. Yu, J. Xiao, and D. Xiao, Phys. Rev. B **98**, 134450 (2018).
  - <sup>31</sup> I. Proskurin, R. L. Stamps, A. S. Ovchinnikov, and J.-i. Kishine, Phys. Rev. Lett. **119**, 177202 (2017).
  - <sup>32</sup> M. W. Daniels, W. Guo, G. M. Stocks, D. Xiao, and J. Xiao, New J. Phys. **17**, 103039 (2015).
  - <sup>33</sup> I. Proskurin, A. S. Ovchinnikov, J.-i. Kishine, and R. L. Stamps, Phys. Rev. B **98**, 134422 (2018).
  - <sup>34</sup> R. Cheng, M. W. Daniels, J.-G. Zhu, and D. Xiao, Sci. Rep. **6**, 24223 (2016).
  - <sup>35</sup> The crucial adjustments in moving from a bipartite to a synthetic antiferromagnet are to send  $-|J_{AFM}|\nabla\mathbf{m}_A \cdot \nabla\mathbf{m}_B \mapsto (|J_{FM}|/2)(|\nabla\mathbf{m}_A|^2 + |\nabla\mathbf{m}_B|^2)$  and  $(D/2)(\mathbf{m}_A \cdot \nabla \times \mathbf{m}_B + \mathbf{m}_B \cdot \nabla \times \mathbf{m}_A) \mapsto (D/2)(\mathbf{m}_A \cdot \nabla \times \mathbf{m}_A + \mathbf{m}_B \cdot \nabla \times \mathbf{m}_B)$ . In the staggered order language, the former amounts to changing the sign of  $\nabla\mathbf{m} \cdot \nabla\mathbf{m}$  in the exchange free energy,

- and the latter amounts to changing the sign of  $\mathbf{n} \cdot (\nabla \times \mathbf{n})$  in the DMI free energy. Except for details of the isospin Hamiltonian  $\mathcal{H}$  in Eq. (5c) arising from the presence of time-reversal plus sublattice exchange symmetry in synthetic antiferromagnets (which is lost in textured bipartite systems), the semiclassical magnon equations of motion (5) are structurally identical between the two cases.<sup>30</sup>
- <sup>36</sup> S. K. Kim, Y. Tserkovnyak, and O. Tchernyshyov, Phys. Rev. B **90**, 104406 (2014).
- <sup>37</sup> E. G. Tveten, A. Qaiumzadeh, O. A. Tretiakov, and A. Brataas, Phys. Rev. Lett. **110**, 127208 (2013).
- <sup>38</sup> D. Culcer, Y. Yao, and Q. Niu, Phys. Rev. B **72**, 085110 (2005).
- <sup>39</sup> R. Shindou and K.-I. Imura, Nuclear Physics B **720**, 399 (2005).
- <sup>40</sup> V. K. Dugaev, P. Bruno, B. Canals, and C. Lacroix, Phys. Rev. B **72**, 024456 (2005).
- <sup>41</sup> K. Y. Guslienko, G. R. Aranda, and J. M. Gonzalez, Phys. Rev. B **81**, 014414 (2010).
- <sup>42</sup> In certain cases where the DMI vector is out of plane, Berry curvature terms may appear in the momentum space equation above. There are explored elsewhere in the literature;<sup>63,64</sup> so here we neglect them and we focus only on the skyrmion-specific phenomenology.
- <sup>43</sup> J. Lan, W. Yu, and J. Xiao, Nat. Comm. **8**, 178 (2017).
- <sup>44</sup> J. Lan, W. Yu, R. Wu, and J. Xiao, Phys. Rev. X **5**, 041049 (2015).
- <sup>45</sup> W. Yu, J. Lan, R. Wu, and J. Xiao, Phys. Rev. B **94**, 140410(R) (2016).
- <sup>46</sup> W. Yu, J. Lan, and J. Xiao, Phys. Rev. B **98**, 144422 (2018).
- <sup>47</sup> P. Yan, X. S. Wang, and X. R. Wang, Phys. Rev. Lett. **107**, 177207 (2011).
- <sup>48</sup> Left-handed spin waves can be found in ferromagnets in principle, but not as low-lying excitations at the energy scales of interest here.
- <sup>49</sup> S. A. Díaz, J. Klinovaja, and D. Loss, Phys. Rev. Lett. **122**, 187203 (2019).
- <sup>50</sup> S. K. Kim, O. Tchernyshyov, and Y. Tserkovnyak, Phys. Rev. B **92**, 020402(R) (2015).
- <sup>51</sup> The unusual  $\sqrt{2}$  factor in our mass tensor compared to that of Tveten *et al.* arises from our direct use of  $S = s\hbar$  in our Berry phase Lagrangian; Tveten *et al.* base their notation directly on the gyromagnetic factor.
- <sup>52</sup> C. Kittel, *Introduction to solid state physics* (Wiley, 2005).
- <sup>53</sup> R. Khoshlahni, A. Qaiumzadeh, A. Bergman, and A. Brataas, Phys. Rev. B **99**, 054423 (2019).
- <sup>54</sup> S. B. Gudnason and C. Halcrow, Phys. Rev. D **98**, 125010 (2018).
- <sup>55</sup> A. A. Serga, A. V. Chumak, and B. Hillebrands, J. Phys. D: Appl. Phys. **43**, 264002 (2010).
- <sup>56</sup> R. Lebrun, A. Ross, S. Bender, A. Qaiumzadeh, L. Baldrati, J. Cramer, A. Brataas, R. Duine, and M. Kläui, Nature **561**, 222 (2018).
- <sup>57</sup> C. L. Hogan, Bell Syst. Tech. J. **31**, 1 (1952).
- <sup>58</sup> R. Fleury, D. L. Sounas, C. F. Sieck, M. R. Haberman, and A. Alù, Science **343**, 516 (2014).
- <sup>59</sup> K. Vogt, F. Fradin, J. Pearson, T. Sebastian, S. Bader, B. Hillebrands, A. Hoffmann, and H. Schultheiss, Nat. Comm. **5**, 3727 (2014).
- <sup>60</sup> A. S. Núñez, R. A. Duine, P. Haney, and A. H. MacDonald, Phys. Rev. B **73**, 214426 (2006).
- <sup>61</sup> Y. Xu, S. Wang, and K. Xia, Phys. Rev. Lett. **100**, 226602 (2008).
- <sup>62</sup> J. M. Gomez-Perez, S. Vélez, L. McKenzie-Sell, M. Amado, J. Herrero-Martín, J. López-López, S. Blanco-Canosa, L. E. Hueso, A. Chuvilin, J. W. A. Robinson, and F. Casanova, Phys. Rev. Appl. **10**, 044046 (2018).
- <sup>63</sup> R. Cheng, S. Okamoto, and D. Xiao, Phys. Rev. Lett. **117**, 217202 (2016).
- <sup>64</sup> V. A. Zyuzin and A. A. Kovalev, Phys. Rev. Lett. **117**, 217203 (2016).